Spatially-resolved measurement on time-dependent electromagnetic behavior in alternating current carrying coated conductor

Higashikawa, Kohei
Department of Electrical Engineering, Graduate School of Information Science and Electrical Engineering, Kyushu University

Honda, Yoshihiro
Department of Electrical Engineering, Graduate School of Information Science and Electrical Engineering, Kyushu University

Inoue, Mitsuteru
Department of Electrical Engineering, Graduate School of Information Science and Electrical Engineering, Kyushu University

Iwakuma, Masataka
Department of Electrical Engineering, Graduate School of Information Science and Electrical Engineering, Kyushu University

他

出版情報：Physica C : Superconductivity and its Applications. 470 (20), pp.1280-1283, 2010-11-01. Elsevier
バージョン：

WT-29 / ISS2009

Submitted 3 November 2009, Revised 13 February 2010

Spatially-resolved measurement on time-dependent electromagnetic behavior in alternating current carrying coated conductor

K. Higashikawa [a,*], Y. Honda [a], M. Inoue [a], M. Iwakuma [a], T. Kiss [a],

K. Nakao [b], Y. Yamada [b], T. Izumi [b]

[a] Department of Electrical Engineering, Graduate School of Information Science and Electrical Engineering, Kyushu University, 744 Motooka, Nishi-ku, Fukuoka 819-0395, Japan

[b] Superconductivity Research Laboratory, International Superconductivity Technology Center, 1-10-13 Shinonome, Koto-ku, Tokyo 135-0062, Japan

Abstract

Establishment of processing technology for multifilamentary coated conductors (CCs) is a key issue for superconducting electric power applications from the viewpoint of AC loss reduction. On the other hand, CCs sometimes have local inhomogeneity in the superconducting layers. In such case, that will cause a current blocking in a filament or inhomogeneity of critical current among filaments in a multifilamentary CC. Therefore, we need an assessment method for local electromagnetic behavior on AC

loss properties of CCs. In this study, we developed a method for visualizing time-dependent AC loss distribution in CCs by using scanning Hall probe microscopy. We succeeded in visualizing local current density, electric field and loss density simultaneously with a spatial resolution of a few hundred micrometers. The measurement system has possible scanning area of 150 x 50 mm^2 and current capacity of 500 A. This enables us to discuss the local electromagnetic behavior on a practical scale of CCs. We believe that this visualization method will be a very powerful tool to estimate the feasibility of processing technology for multifilamentary CCs.

PACS codes: 74.72.Bk, 74.25.Nf, 84.71.Mn

Keywords: visualization; AC loss; coated conductor; magnetic microscopy

* Corresponding Author.

Dr. Kohei Higashikawa

Postal address: Kiss Laboratory, Department of Electrical and Electronic Systems Engineering, Graduate School of Information Science and Electrical Engineering, Kyushu University, 744 Motooka, Nishi-Ku, Fukuoka 819-0395, Japan

Tel: +81-92-802-3678

Fax: +81-92-802-3677

E-mail: kohei@super.ees.kyushu-u.ac.jp

1. Introduction

Fabricating processes of $REBa_2Cu_3O_{7-\delta}$ (REBCO, RE: rare earth) coated conductors (CCs) such as $YBa_2Cu_3O_{7-\delta}$ (YBCO) and $GdBa_2Cu_3O_{7-\delta}$ (GdBCO) CCs have been developed steadily in recent years [1-4]. For example, SuperPower Inc. has achieved a 1065 m long CC with the minimum critical current of 282 A/cm [4]. Such a progress leads us to the next stage of the development of practical applications using CCs.

For electric power applications, on the other hand, forming multifilamentary configuration on CCs will also be a key technology from the point of view of AC loss reduction. For example, it has been reported that AC losses in CCs can be reduced by increasing the number of filaments [5-8]. This demonstrates the high applicability of CCs to electric power applications such as power transmission cables, transformers and superconducting magnetic energy storage.

However, it has also been reported that CCs sometimes have local defects and inhomogeneity in the superconducting layers [9, 10]. In case of monofilamentary CCs, e.g., 10-mm-wide CCs, that does not largely influence the total performance because current can flow around such defects. In case of multifilamentary CCs, on the other hand, that will cause a significant current blocking in a filament or inhomogeneity of critical current among filaments. In such cases, we cannot discuss the electromagnetic

behavior only from a general AC loss estimation such as the four-probe method and pick-up coil method because we can only detect global loss integrating whole period. Therefore, for the establishment of the processing technology for multifilamentary CCs, we need an assessment method to understand the local electromagnetic behaviors on AC loss properties of CCs.

In this study, we developed a visualization method of time-dependent AC loss distribution in CCs by using scanning Hall probe microscopy. We tried to visualize local current density, electric field and loss density in a multifilamentary model sample of a YBCO CC under alternating transport current.

2. Methods

2.1. Sample

Fig. 1 shows an optical micrograph of the sample. The sample was prepared from a 10-mm-wide YBCO CC, and was processed by photolithography and wet etching. 10 filaments were patterned on a 5-mm-wide and 8-mm-long area, and the width of each filament was 340 μm. Furthermore, some failures such as bridges, disconnections and defects were purposely simulated on the sample. We used this sample as an example for the visualization method.

2.2. Measurement

Fig. 2 shows a schematic diagram of the measurement system. The system of the scanning Hall probe microscopy has two liquid nitrogen tanks. One is for current leads, and this enables current capacity of 500 A. The other is for cooling stage. The sample is cooled by heat conduction from the stage, and then a typical temperature of the stage becomes around 82 K. The Hall probe is located above the sample. The active area of the Hall sensor is 50 μm x 50 μm, and perpendicular component of magnetic field, B_z, generated by the sample is measured by this sensor. The Hall probe can be controlled with a spatial resolution of 1 μm, 1 μm and 0.25 μm in *x*, *y* and *z* directions, respectively.

A sinusoidal transport current was applied to the sample from a bipolar current source controlled by a function generator. For noise reduction, also the Hall sensor was biased by another channel of the function generator, and then the signal from the sensor was acquired through a lock-in amplifier. At a measurement point, B_z was measured during one cycle of the alternating transport current by synchronizing the transport current. Then, the Hall probe was moved to the next measurement point. These procedures were repeated for a whole measurement area, and eventually we could obtain in-plane distributions of B_z as a function of time.

2.3. Data analysis

If we assume in-plane 2D current distribution in the sample, i.e., sheet current density in *xy*-plane, ***J***, the distribution of ***J*** can be derived analytically from that of measured B_z based on the inverse problem of Biot-Savart law. Roth et al. have already reported a method for that, and *x* and *y* components of ***J***, J_x and J_y, are expressed in Fourier space as follows [11]:

$$\tilde{J}_x(k_x,k_y) = -i\frac{2}{\mu_0}\frac{k_y}{k}e^{kz_{\text{lift-off}}}\tilde{B}_z(k_x,k_y) \quad (1)$$

$$\tilde{J}_y(k_x,k_y) = i\frac{2}{\mu_0}\frac{k_x}{k}e^{kz_{\text{lift-off}}}\tilde{B}_z(k_x,k_y) \quad (2)$$

where $\tilde{J}_x$, $\tilde{J}_y$ and $\tilde{B}_z$ are the Fourier transformations of J_x, J_y and B_z, respectively. The variables k_x and k_y are the components of the wave number ***k***, and *k* is the absolute value of ***k*** given by $\sqrt{k_x^{\,2}+k_y^{\,2}}$. The constant $z_{\text{lift-off}}$ is the distance from the current sheet to the measurement point of B_z. According to the increment of $z_{\text{lift-off}}$, spatial harmonics of $\tilde{B}_z$ are weakened especially at large *k*. Eqs. (1) and (2) indicate that such harmonics should be amplified by the term of $e^{kz_{\text{lift-off}}}$ to restore the magnetic field just at the current sheet. However, at very large *k*, the harmonics are weakened down to a noise level of the measurement. This means that we should give up the information of such large *k*. Therefore, some low-pass filter should be used, and the Hanning window was used in this study. The cut-off wavelength, $\lambda_{\text{cut-off}}$, determines the spatial resolution of the distribution of ***J***.

Furthermore, the distribution of electric field, $\boldsymbol{E}$, can also be estimated from that of the time-derivative B_z based on Faraday's Law. Dinner et al. have reported a method for that [12], and x and y components of $\boldsymbol{E}$, E_x and E_y, are expressed in Fourier space as follows:

$$\tilde{E}_x(k_x,k_y) = i\frac{k_y}{k^2}e^{kz_{\text{lift-off}}}\frac{\partial\tilde{B}_z(k_x,k_y)}{\partial t} \tag{3}$$

$$\tilde{E}_y(k_x,k_y) = -i\frac{k_x}{k^2}e^{kz_{\text{lift-off}}}\frac{\partial\tilde{B}_z(k_x,k_y)}{\partial t} \tag{4}$$

where $\tilde{E}_x$ and $\tilde{E}_y$ are the Fourier transformations of E_x and E_y, respectively. However, Eqs. (3) and (4) are valid only when the curl-free electrostatic portion, $\boldsymbol{E}_p$, is negligible compared with the divergence-free inductive $\boldsymbol{E}_i$ [12]. In this study, the transport current applied to the sample was 88% of the critical current of the sample at the maximum. In case of a typical CC, the corresponding electric field in steady state, i.e., the magnitude of $\boldsymbol{E}_p$, becomes two orders smaller than the electric field criterion. On the other hand, as a result of the measurement, the magnitude of $\boldsymbol{E}_i$ became the same order as the electric field criterion. Therefore, we did not consider $\boldsymbol{E}_p$, and used Eqs. (3) and (4) for the estimation of the distribution of $\boldsymbol{E}$.

In this way, we can estimate the distributions of $\boldsymbol{J}$ and $\boldsymbol{E}$ from the measurement of B_z. That means that we can finally obtain loss density, q, by considering the inner product of $\boldsymbol{J}$ and $\boldsymbol{E}$:

$$q = J_x E_x + J_y E_y . \tag{5}$$

3. Results and discussion

Fig. 3 shows the distributions of measured magnetic field, sheet current density, electric field and loss density as a function of time. An alternating transport current, I, with an amplitude of 30 A was applied to the sample in x direction with a frequency of 2 Hz. The critical current, I_c, of the sample defined with the electric field criterion of 0.1 mV/m (1 μV/cm) was 34 A at this temperature. Therefore, the maximum load factor (I / I_c) was 88% for these results. The time, t, is defined as zero at the zero phase of the transport current, and then the time cycle becomes 500 ms. Furthermore, these images were obtained with $\lambda_{cut\text{-}off}$ = 230 μm.

A positive current flowing in x direction should generate a positive value of B_z in the upper region and a negative value of B_z in the lower region. Such distributions of B_z were obtained at t > 70 ms. However, the situation was opposite at t < 30 ms in the middle part of the sample while the total transport current was positive in x direction. For this sample, all filaments were coupled because they were connected with each other at both ends of the sample. Therefore, it can be understood that such opposite distributions are formed as a result of magnetic flux trapped from a negative transport current in the previous cycle of the alternating transport current. This kind of trap can also be confirmed from the fact that B_z keep similar distribution in the middle part of the sample at t > 120 ms while the transport current largely decreases from the peak value.

Such superconducting properties are also well shown in the distributions of the absolute value of sheet current density, J. When the transport current increases at $t <$ 125 ms, the current flows from the uppermost and the lowermost filaments. On the other hand, when the transport current decreases at $t >$ 125 ms, the current disappears from such filaments. This can also be interpreted from the coupling of the filaments. Furthermore, it should be noted that circling current is induced in disconnected or defected filaments. In other words, although such filaments cannot transport enough current, they might generate additional AC losses. That will be discussed in the distributions of q.

From the distributions of the absolute value of electric field, E, it is found that large electric field is induced around t = 70 ms. However, time variation of the transport current is maximum at t = 0 ms (and t = 250 ms). As stated above, magnetic flux are trapped for a while inside the sample. Then, the time variation of magnetic field delays from that of transport current. This is the reason of the difference between them. Furthermore, comparing the distributions of E between t = 6 ms and t = 30 ms, it is found that electric field invades by skipping the disconnected filaments. Such filaments can contribute neither to trap magnetic field in the sample nor to shield magnetic field from outside. Then, magnetic field cannot keep the same value around such filaments. This is the reason of the abovementioned time variation. On the other hand, electric field is very small at $t >$ 120 ms, and this can also be interpreted from the field trap.

Finally, we could obtain the distributions of q. The time variation of the distribution has the same tendency as that of E; Large loss is generated around t = 70 ms, and small loss at t > 120 ms. Furthermore, it is also found that the abovementioned circling current does not generate significant AC losses. In this way, this visualization method enables us to discuss the local electromagnetic behavior in a CC on the AC loss.

4. Conclusion

We developed a visualization method of local electromagnetic behavior in an alternating current carrying CC by using scanning Hall probe microscopy. We succeeded in visualizing sheet current density, electric field and loss density simultaneously with a spatial resolution of a few hundred micrometers as a function of time. Furthermore, we discussed the electromagnetic behavior in detail for a multifilamentary model sample of a YBCO CC. The measurement system had large scanning area and current capacity, and thus we could discuss such local electromagnetic behaviors on a practical scale of the CC. Therefore, we believe that this visualization method will be a powerful assessment technique for the establishment of processing technology for multifilamentary CCs.

Acknowledgments

This work was supported by the ”New Energy and Industrial Technology Development Organization (NEDO) as the Project for Development of Materials & Power Application of Coated Conductors, M-PACC”, “JSPS: KAKENHI (20360143)” and “JSPS: KAKENHI (20.01945)”.

References

[1] V. Selvamanickam, Y. Chen, X. Xiong, Y. Y. Xie, M. Marchevsky, A. Rar, Y. Qiao, R. M. Schmidt, A. Knoll, K. P. Lenseth, C. S. Weber, IEEE Trans. Appl. Supercond. 19 (2009) 3225.

[2] SuperPower Inc., Press Releases (http://www.superpower-inc.com/content/superpower-reports-latest-achievements-2009-u-s-department-energy-peer-review) (2009, August 18).

[3] Y. Shiohara, M. Yoshizumi, T. Izumi, Y. Yamada, Supercond. Sci. Technol. 21 (2008) 034002.

[4] Fujikura Ltd. News Release (http://www.fujikura.co.jp/newsrelease/1194905_2220.html) (2008, December 9).

[5] C. B. Cobb, P. N. Barnes, T. J. Haugan, J. Tolliver, E. Lee, M. Sumption, E. Collings,

C. E. Oberly, , Physica C 382 (2002) 52.

[6] N. Amemiya, S. Kasai, K. Yoda, Z. Jiang, G. A. Levin, P. N. Barnes, C. E. Oberly, Supercond. Sci. Technol. 17 (2004) 1464.

[7] H. Okamoto, H. Hayashi, A. Tomioka, M. Konno, M. Owa, A. Kawagoe, F. Sumiyoshi, M. Iwakuma, K. Suzuki, T. Izumi, Y. Yamada, Y. Shiohara, Physica C 468 (2008) 1731.

[8] K. Suzuki, J. Matsuda, M. Yoshizumi, T. Izumi, Y. Shiohara, M. Iwakuma, A. Ibi, S. Miyata, Y. Yamada, Supercond. Sci. Technol. 20 (2007) 822.

[9] M. Inoue, K. Abiru, Y. Honda, T. Kiss, Y. Iijima, K. Kakimoto, T. Saitoh, K. Nakao, Y. Shiohara, IEEE Trans. Appl. Supercond. 19 (2009) 2847.

[10] K. Abiru, Y. Honda, M. Inoue, T. Kiss, Y. Iijima, K. Kakimoto, T. Saitoh, K. Nakao, Y. Shiohara, Physica C 469 (2009) 1450.

[11] B. J. Roth, N. G. Sepulveda, J. P. Wikswo Jr, J. Appl. Phys. 65 (1989) 361.

[12] R. B. Dinner, K. A. Moler, D. M. Feldmann, M. R. Beasley, Phys. Rev. B 75 (2007) 144503.

Figure Captions

Fig. 1. Optical micrograph of the sample. 10 filaments were patterned on a YBCO coated conductor. The widths of the filament and the gap were 340 μm and 160 μm, respectively. Furthermore, some failures such as bridges, disconnections and defects were intentionally simulated on the sample

Fig. 2. Schematic diagram of the measurement system using the scanning Hall probe microscopy. The current capacity of the system is 500 A. The active area of the Hall sensor is 50 μm x 50 μm, and the probe can be controlled with a spatial resolution of 1 μm, 1 μm and 0.25 μm in *x*, *y* and *z* directions, respectively.

Fig. 3. Experimental results on the distributions of magnetic field, sheet current density, electric field and loss density in the sample as a function of time.

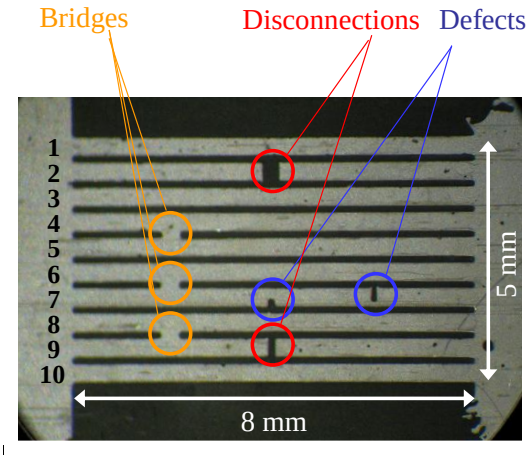
Bridges
Disconnections
Defects
1
2
3
4
5
6
7
8
9
10
5 mm
8 mm

Fig. 1

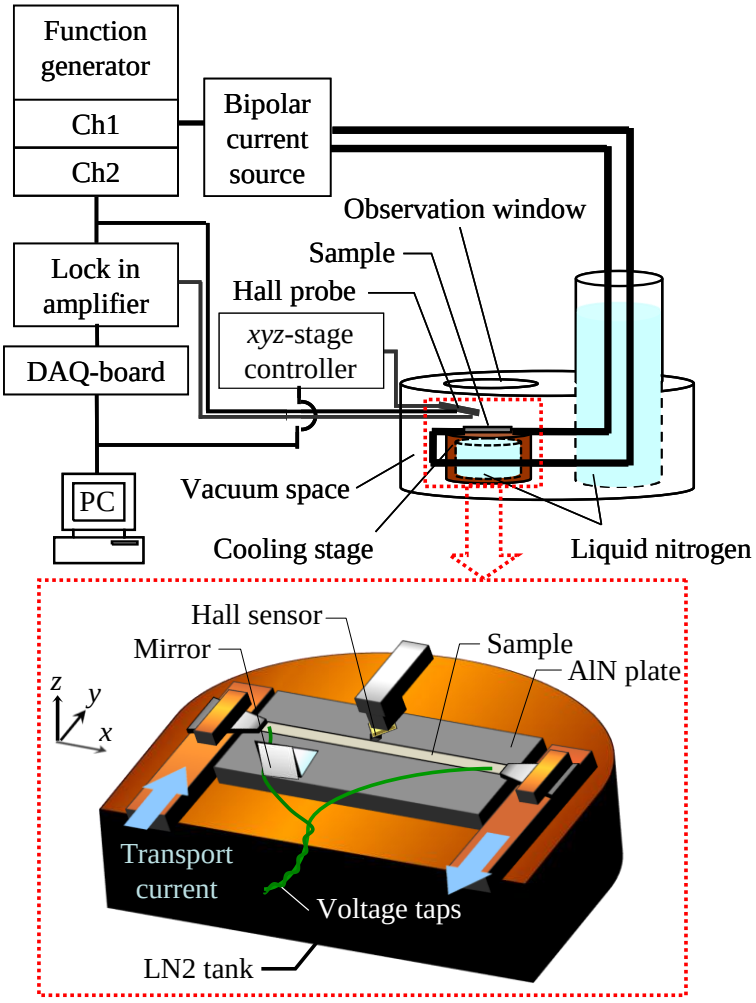
Function generator
Ch1
Ch2
Bipolar current source
Observation window
Sample
Hall probe
Lock in amplifier
xyz-stage controller
DAQ-board
PC
Vacuum space
Cooling stage
Liquid nitrogen
Hall sensor
Mirror
Sample
AlN plate
z
y
x
Transport current
Voltage taps
LN2 tank

Fig. 2

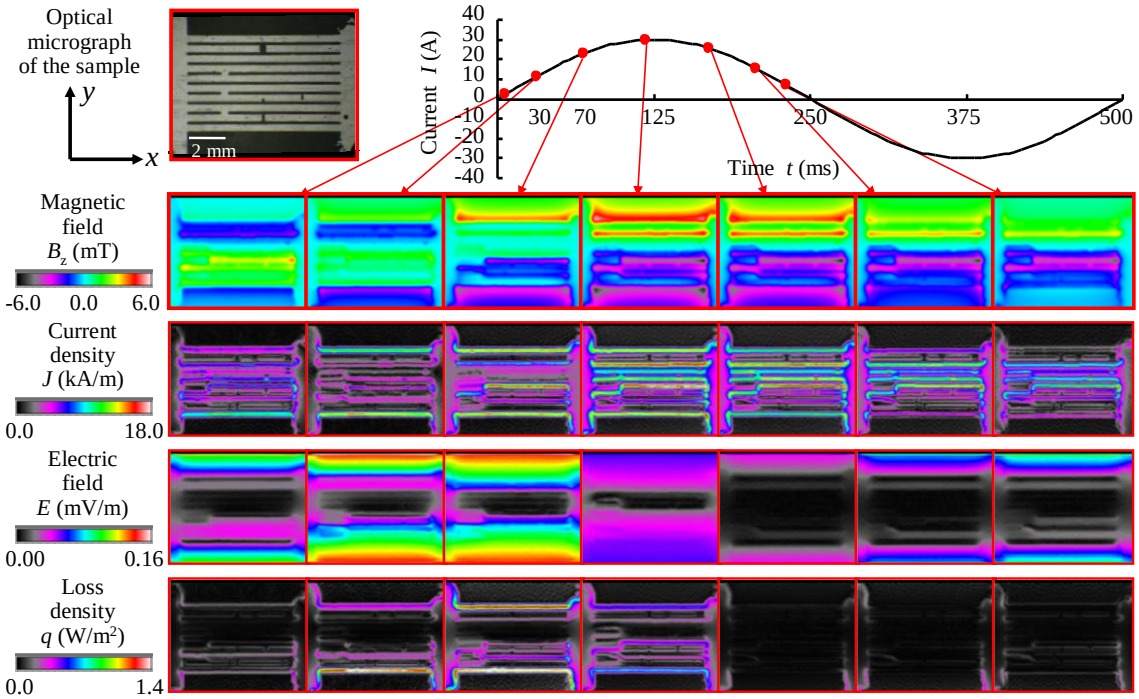
Optical micrograph of the sample
y
x
2 mm
Current I (A)
40
30
20
10
0
-10
-20
-30
-40
30
70
125
250
375
500
Time t (ms)
Magnetic field B_z (mT)
-6.0
0.0
6.0
Current density J (kA/m)
0.0
18.0
Electric field E (mV/m)
0.00
0.16
Loss density q (W/m²)
0.0
1.4

Fig. 3